Short communication

Synthesis and characterization of nanosized lithium manganate and its derivatives

Muhammad Javed Iqbal [*], Sabia Zahoor

Department of Chemistry, Quaid-i-Azam University, Islamabad 45320, Pakistan

Abstract

Spinel lithium manganese oxide, $LiMn_2O_4$ and its derivatives are prepared by the sol–gel method. The lattice constant of the pure material is calculated as 8.23 Å. Different transition metal cations of chromium, iron, cobalt, nickel, copper and zinc (0.05 and 0.15 M) are doped in place of manganese in the $LiMn_2O_4$. X-ray powder diffraction data show that the spinel framework preserved its integrity upon doping. Formation of a single phase and the purity of the samples are confirmed by X-ray powder diffraction (XRD) and Fourier-transform infrared spectroscopy (FTIR). The crystallite size of the samples is calculated by use of the Scherrer formula and is found to be within a range of 43–66 nm. The electrical conductivity of the samples is determined over a temperature range of 200–300 K by means of four-point probe method. An increasing trend of conductivity with increase in temperature is noted for all the samples. The parent compound $LiMn_2O_4$ has a conductivity value of 3.47×10^{-4} ohm^{-1} cm^{-1} at room temperature. This value increases on doping with the above-mentioned transition metal cations.
© 2006 Elsevier B.V. All rights reserved.

Keywords: Lithium manganate; Nanoparticles; Electrical conductivity; Crystallite size; Lithium–ion battery; Transition metal doping

1. Introduction

Nanosized materials have attracted much attention in various fields of chemistry and physics during the past two decades [1,2]. The interest in nanoscale materials arises from the fact that the optical, electrical, mechanical, electronic and chemical properties of the materials are a function of their dimensions. In this size regime, it is found that as the particle becomes smaller, the semiconductor energy levels become more separated from each other and the effective band-gap increases [3]. It has been shown [4] that nanocrystalline metal oxide semiconductor films and electrodes often possess superior charge-transport and/or charge-storage characteristics.

The unique properties of these nanoparticle semiconductors have resulted in their potential applications in many areas such as microelectronics, photovoltaics, imaging and display technologies, sensing devices and thin-film coatings. Lithium manganese spinels have been extensively investigated as poitive electrode materials for lithium–ion batteries due to their high theoretical energy density, inexpensive material cost, environmental friendliness and good safety [5–8]. The preparation and characteristics of nanocrystalline $Li_{1+x}Mn_{2-x}O_4$ spinels have been described in the recent past [9,10] but their crystallite sizes were located within the micrometer scale. A large surface area to volume ratio is expected to be found in metallic nanoparticles, which permits effective charge-transfer [11] and therefore nanoparticles may prove to be good positive electrode (cathode) materials.

The classical method of synthesis of spinel $LiMn_2O_4$ materials via a solid-state reaction using lithium carbonate and manganese oxides has been used extensively [12,13], but it requires a prolonged heat treatment at relatively high temperatures with repeatedly intermediate grinding. Moreover, this method does not provide good control of crystalline growth, compositional homogeneity, morphology, and microstructure. As a consequence, the final products consist of relatively large particles ($>1 \mu m$) with a broad particle-size distribution. In order to overcome these disadvantages, sol–gel [14], xero–gel [6], pechini [7,8], freeze-drying [9] and emulsion-drying [10] preparative techniques have been developed. These methods produce homogenous spinel materials with nanosized particles.

In the present study, the sol–gel method has been employed to prepare nanocrystalline $Li_{1+x}Mn_{2-x}O_4$ ($x = Cr$, Fe, Co, Ni,

---

[*] Corresponding author. Tel.: +92 51 9219811; fax: +92 51 2873869.
E-mail address: mjiqauchem@yahoo.com (M.J. Iqbal).

Cu and Zn) compounds. These are annealed in air at two different temperatures, i.e., 873 and 1073 K, in order to examine the effect of annealing temperature on crystallinity and particle size. The samples are characterized by X-ray powder diffraction for analysis of the crystalline phase, particle size and morphology. The electrical conductivity is measured by the usual four-point probe method [11,12].

2. Experimental

All the materials used in the synthesis were high-purity compounds, namely: manganese acetate tetrahydrate (Merck, 99.9%), lithium nitrate (Fluka, >98%), nickel acetate (Merck, 98%), chromium nitrate (Riedel-Dehaen, 99%), iron nitrate·$9H_2O$ (Panrreac, 98%), zinc acetate (Fluka, 99%), cobalt acetate (Fluka, 98%), ethylene glycol (BDH, 99%) and methanol (Riedel-Dehaen, 99.8%). The compounds were used as supplied.

The sol–gel method was employed for the preparation of the samples in which 4.569 g of $LiNO_3$ and 24.509 g of $Mn(CH_3COO)_2 \cdot 4H_2O$ were dissolved in a solution of 12 ml of ethylene glycol and 36 ml of methanol, i.e., in a volumetric ratio of 1:3. The resulting mixture was refluxed at 353 K for 12 h. The solvent was evaporated at 393 K, using a hot plate with a magnetic stirrer, until the formation of a gel. This was converted to a powder that was then annealed in a temperature programmed tube furnace at 1073 K at a heating rate of 5 °C per min and a cooling rate of 5 °C per min. All other samples were prepared via same procedure, except that a stoichiometric amount of dopants was included at the initial stage. The nitrates or acetates of Cr, Fe, Co, Ni, Cu and Zn as dopants were used as precursors and two different concentrations (0.05 and 0.15 M) of each dopant was taken. All samples were annealed at 873 or 1073 K with the same heating and cooling rates.

The phase composition, morphology and particle size of each sample was analysed by powder X-ray diffractometry (XRD) with a Philips PW 3040 instrument that employed Cu Kα radiation. Data were collected in the 2θ range 5° to 90° with a step interval of 0.04° and a counting time of 1 s per step. The lattice parameters were determined by the least-squares method using several diffraction peaks. The four-point probe method [15] was employed to determine the electrical conductivity of the samples within a temperature range of 200–300 K using a liquid nitrogen cryostat system (Janis Research Model IC-35D LN2) in conjunction with a multimeter (Kiethley 2400) that served as a constant-current source meter. A second multimeter was used to read voltage and a PT100 thermocouple measured the temperature with an accuracy of ±0.001 K. The accuracy of measurement of electrical resistivity was ±0.01 Ω^{-1} cm^{-1}.

3. Results and discussions

3.1. Phase analysis

The infrared spectra of pure and doped $LiMn_2O_4$ (frequency range 4000–400 cm^{-1}) are shown in Figs. 1 and 2. Two main absorption bands are observed at 511 and 613 cm^{-1} in both compounds and are due to the asymmetric stretching modes of MnO_6
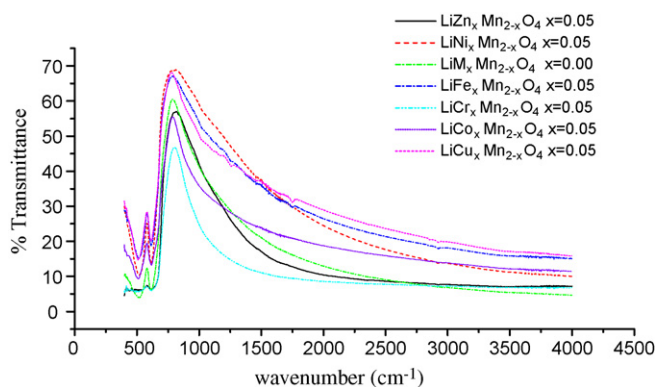

Fig. 1. FTIR spectra of $LiM_xMn_{2-x}O_4$ annealed at 873 K where M = Cr, Fe, Co, Ni, Cu, Zn and x = 0.00, 0.05.

group (absorption due to spinel framework) [16]. The very minor absorption peaks at 2310 and 2370 cm^{-1} are believed to represent CO_2, the bands at 1760 and 1800 cm^{-1} appear to arise form the stretching vibration of the C=O bond of CH_3COOH, and the absorption at 1190 cm^{-1} is associated with the C–O vibration of the acetic acid. The stretching vibration of the O–H bond appears above 3500–3800 cm^{-1} [17]. The absorption bands around 1450–1750 cm^{-1} and above 3500 cm^{-1} are assigned to water absorption. It is noted that only the samples annealed at 873 K (Fig. 1) exhibit CO_2 vibration (peak at 2336 cm^{-1}) and water absorption (peak above 3500 cm^{-1}). Whereas, the samples annealed at 1073 K do not display either of these absorption peaks (Fig. 2). Also, no absorption bands at 2310–2370 cm^{-1}, 1190 cm^{-1}, or above 3500 cm^{-1} are observed in any of the samples. This clearly demonstrates that no unreacted precursor, i.e., nitrates and acetates, used in the preparation of $LiMn_2O_4$ and its derivatives are present in the final materials produced at 1073 K.

Fig. 3(a) shows the XRD pattern of $LiMn_2O_4$ synthesized by the sol–gel method. Very sharp and high intensity peaks with $h k l$ value of (1 1 1), (3 1 1), (2 2 2), (4 0 0), (3 3 1), (5 1 1), (4 4 0) and (5 3 1) are present and correspond to the cubic phase of $LiMn_2O_4$ (JCPDS 35-782). Figs. 3 and 4 show the XRD patterns of $LiM_xMn_{2-x}O_4$, where M = Cr, Fe, Co, Ni, Cu and Zn, annealed at 873 and 1073 K, respectively. No sign of impurity phases is observed and all the peaks are indexed to the cubic spinel (JCPDS 35-782) of the space group Fd3m. Thus, a single
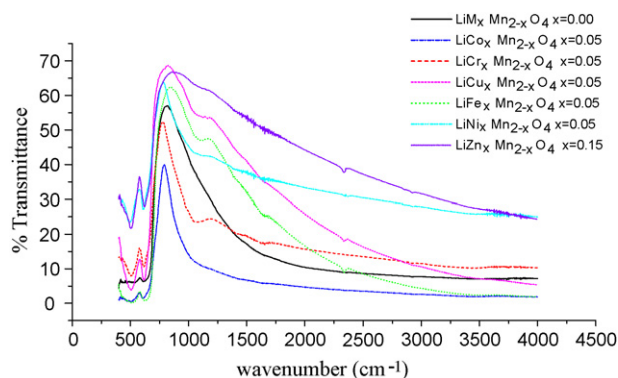

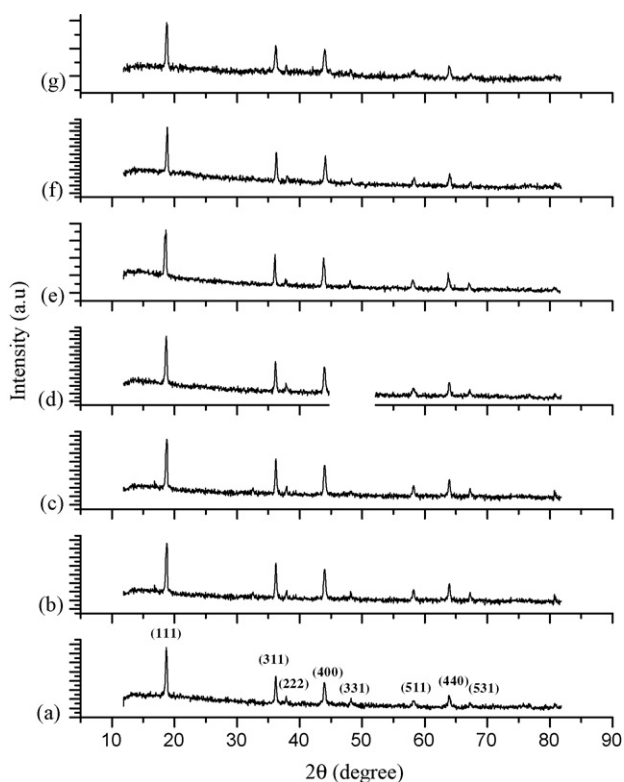Fig. 2. FTIR spectra of $LiM_xMn_{2-x}O_4$ annealed at 1073 K where M = Cr, Fe, Co, Ni, Cu, Zn and x = 0.00, 0.05.

Fig. 3. XRD pattern of: (a) $LiMn_2O_4$, (b) $LiCr_{0.05}Mn_{1.95}O_4$, (c) $LiFe_{0.05}Mn_{1.95}O_4$, (d) $LiCo_{0.05}Mn_{1.95}O_4$, (e) $LiNi_{0.05}Mn_{1.95}O_4$, (f) $LiCu_{0.05}Mn_{1.95}O_4$, (g) $LiZn_{0.05}Mn_{1.95}O_4$ annealed at 873 K.
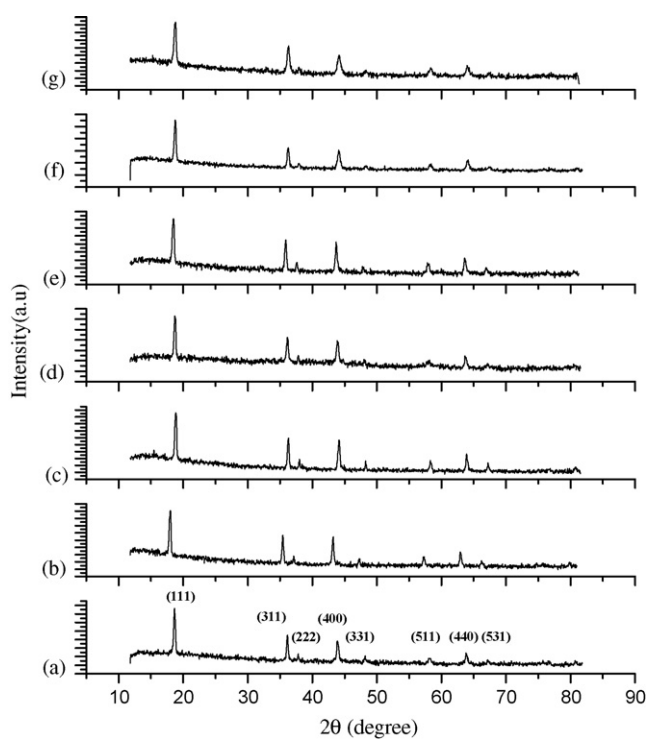
Fig. 4. XRD pattern of: (a) $LiMn_2O_4$, (b) $LiCr_{0.05}Mn_{1.95}O_4$, (c) $LiFe_{0.05}Mn_{1.95}O_4$, (d) $LiCo_{0.05}Mn_{1.95}O_4$, (e) $LiNi_{0.05}Mn_{1.95}O_4$, (f) $LiCu_{0.05}Mn_{1.95}O_4$, (g) $LiZn_{0.05}Mn_{1.95}O_4$ annealed at 1073 K.

Table 1
Comparison of crystallite sizes of various samples annealed at 873 and 1073 K

Samples	Crystallite sizes of the samples annealed at 873 K (nm)	Crystallite sizes of the samples annealed at 1073 K (nm)
$LiMn_2O_4$	31	32
$LiCr_{0.05}Mn_{1.95}O_4$	52	54
$LiFe_{0.05}Mn_{1.95}O_4$	41	44
$LiCo_{0.05}Mn_{1.95}O_4$	52	54
$LiNi_{0.05}Mn_{1.95}O_4$	59	64
$LiCu_{0.05}Mn_{1.95}O_4$	52	59
$LiZn_{0.05}Mn_{1.95}O_4$	52	59

phase of spinel $LiMn_2O_4$ has been formed. Peak (1 1 1) appears as the strongest peak in all the samples (relative intensity = 100). This shows that Li^+ occupies the tetrahedral (8a) site, and thus, the sample is a normal spinel. The absence of peak (2 2 0) in all the samples ensures the absence of inverse spinel as this peak appears only in case of cations in the tetrahedral site [17]. Although, the dopants investigated here are of comparable size to Mn [18], the shift in peak position is attributed to the effect of small differences in the doped cation size.

3.2. Lattice parameter and cell volume

The average lattice parameters "a" of the samples are given in Table 2. The change in the lattice parameters and the cell volumes can be attributed to changes in the ionic radii of the doped cations [18]. The increase in lattice parameter in the order $Ni^{2+} < Co^{2+} < Fe^{3+} < Mn^{3+} < Cr^{3+} < Cu^{2+} < Zn^{2+}$, as shown in Fig. 5, is in correspondence with the ionic radii of these cations, i.e., Ni^{2+} (0.62 Å) $< Co^{2+}$ (0.63 Å) $< Fe^{3+}$ (0.64 Å) $< Mn^{3+}$ (0.66 Å) $< Cr^{3+}$ (0.69 Å) $< Cu^{2+}$ (0.70 Å) $< Zn^{2+}$ (0.74 Å) (Table 1).

The increase in the lattice parameter and cell volume of the $LiMn_2O_4$ spinel unit cell caused by various dopants, i.e., Cr^{3+}, Zn^{2+}, is because the radii of Cr^{3+} (0.69 Å) and Zn^{2+} (0.74 Å) are larger than that of Mn^{3+} (0.66 Å). The lattice constant and the cell volume of the Li–Mn–O spinel compound is found to decrease with substitution of iron, cobalt and nickel which may be due to the smaller sizes of the substituting Fe^{3+} (0.64 Å), Ni^{2+} (0.62 Å) and Co^{2+} (0.63 Å) compared with larger Mn^{3+} ion. Also, cobalt ion has a greater binding energy (1067 kJ mol^{-1}) in the CoO_6 octahedra than the Mn ion in the MnO_6 octahedra (946 kJ mol^{-1}) [19]. It is therefore assumed that the Co^{2+} ion substitutes the Mn sites homogenously while retaining the Fd3m space group. Similarly, Ni^{2+} is expected to replace Mn^{3+} in $LiNi_xMn_{2-x}O_4$ material. As manganese exists both as Mn^{3+} and Mn^{4+} in $LiMn_2O_4$, some of the Mn^{3+} ions would be expected to change into Mn^{4+} in order to maintain electroneutrality upon doping with Ni^{2+}. Since Mn^{4+} has a small size (0.54 Å) compared with Mn^{3+} (0.66 Å), this factor should be responsible for the observed decrease in the cell constant of nickel-doped samples. Although Cu^{2+} (0.70 Å) has a larger ionic radius than that of Mn^{3+}, there is a difference of one positive charge in case of Cu^{2+} so in order to maintain overall electroneutrality more of the Mn^{3+} would be changed into Mn^{4+} upon doping

Table 2
Comparison of average lattice parameter and cell volume of samples annealed at 873 and 1073 K

Samples	Average lattice parameter "a" (Å) at 873 K	Average lattice parameter "a" (Å) at 1073 K	Average cell volume (Å^3) at 873 K	Average cell volume (Å^3) at 1073 K
$LiMn_2O_4$	8.21	8.23	565	557
$LiCr_{0.05}Mn_{1.95}O_4$	8.22	8.24	567	559
$LiFe_{0.05}Mn_{1.95}O_4$	8.20	8.23	565	557
$LiCo_{0.05}Mn_{1.95}O_4$	8.20	8.22	563	555
$LiNi_{0.05}Mn_{1.95}O_4$	8.19	8.21	561	553
$LiCu_{0.05}Mn_{1.95}O_4$	8.23	8.26	571	563
$LiZn_{0.05}Mn_{1.95}O_4$	8.25	8.28	575	567

with Cu^{2+} and hence the lattice constant is not increased that much.

3.3. Effect of annealing temperature

All the samples were annealed at 873 and at 1073 K. In addition to the peaks corresponding to cubic spinel structure, there appears a minor peak in the samples annealed at 873 K, which was identified as Mn_2O_3 [20,21] as shown in Fig. 3. On increasing the annealing temperature from 873 to 1073 K, the peak intensity of $LiMn_2O_4$ is increased while the impurity phase Mn_2O_3 disappears almost completely (Fig. 4). Lithium manganese oxide with well-developed crystallinity is obtained by annealing at 1073 K for 24 h at a heating rate of 5 °C per min.

The variation of crystallite size with annealing temperature is evident from the data given in Table 1. The samples annealed at 873 K consist of crystallites of small size but with increase in annealing temperature from 873 to 1073 K, the crystallite size of pure $LiMn_2O_4$ as well as of samples doped with chromium, nickel, copper and zinc increases significantly, perhaps due to sintering of smaller particles to form aggregates. The lattice constants and the cell volume of $LiMn_2O_4$ and its derivatives calculated from XRD data are also listed in Table 2. A slight increase in the lattice constant for all the samples annealed at 1073 K indicates that the Mn^{4+} content in Li–Mn–O spinel is higher at this annealing temperature. This is because the ionic radius of Mn^{4+} (0.54 Å) is lower than that of Mn^{3+} (0.66 Å) and Mn^{4+} is less stable at higher temperature [22] so the Mn^{3+} content increases on raising the annealing temperature from 873 to 1073 K.

3.4. Electrical conductivity

The measured value of the electrical conductivity of various samples is of the order of $10^{-4}\ \Omega^{-1}\ cm^{-1}$ at room temperature and this falls within the semiconductor range (10^{-10} to $10^{-4}\ \Omega^{-1}\ cm^{-1}$). The $LiMn_2O_4$ samples exhibit an increase in electrical conductivity with increase in temperature, as shown in Figs. 6 and 7. A finite amount of energy is necessary to violate Anderson's condition, and thus make an electron move from one atom to other [23].

The electrical conductivity of $LiMn_2O_4$ is improved with increase in the calcination temperature. For instance, the conductivity of samples annealed at 873 K is $3.20 \times 10^{-4}\ \Omega^{-1}\ cm^{-1}$ and of those annealed at 1073 K is $4.17 \times 10^{-4}\ \Omega^{-1}\ cm^{-1}$
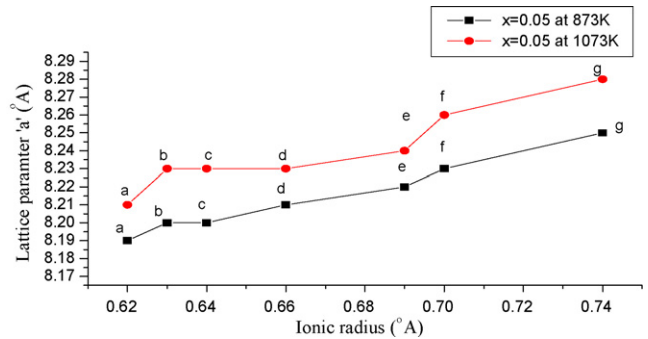
Fig. 5. Lattice paprameter as a function of ionic radii: (a) Ni^{2+}, (b) Co^{2+}, (c) Fe^{3+}, (d) Cr^{3+}, (e) Cu^{2+} and (f) Zn^{2+}.

(Table 3). The improvement is due to: (i) the better structural ordering that may have taken place at the higher calcination temperature of 1073 K; (ii) the higher concentration of the effective charge carriers i.e., [Mn^{3+}] and [Mn^{4+}]. The electrical conduction in $LiMn_2O_4$, is through a small polaran Mn^{3+}, i.e., via hopping of electrons between e_g orbitals on adjacent Mn^{3+}/Mn^{4+}. Unpaired electrons from the e_g orbitals of high spin Mn^{3+} (d^4) hop to neighbouring low spin Mn^{4+} (d^3) ions. Both the e_g orbitals of the metal ion lie on the same site so these are equivalent in energy and hopping is limited to orbitals of the same energy [24].

The electrical conductivity of $LiMn_2O_4$ is improved by the addition of Cr^{3+}, Co^{2+}, Ni^{2+}, Cu^{2+} and is decreased by the addition of Fe^{3+}, Zn^{2+}, as shown in Table 3. $LiMn_2O_4$ is known to
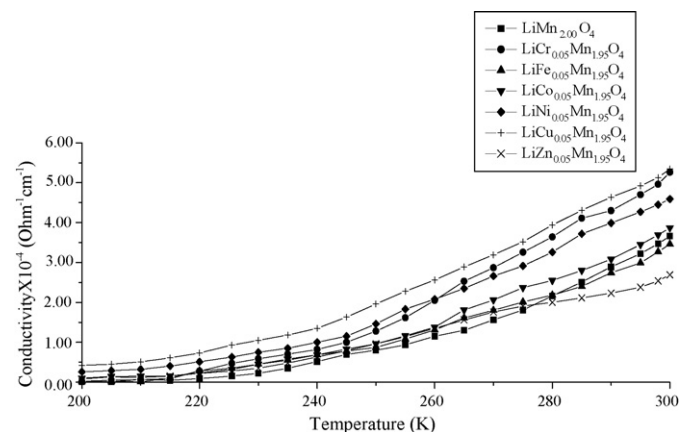

Fig. 6. Conductivity pattern of $LiM_xMn_{2-x}O_4$ synthesized by sol–gel method and annealed at 873 K where $x = 0.05$ and M = Cr, Fe, Co, Ni, Cu and Zn.

Fig. 7. Conductivity pattern of $LiM_xMn_{2-x}O_4$ synthesized by sol–gel method and annealed at 1073 K where $x = 0.05$ and M = Cr, Fe, Co, Ni, Cu and Zn.
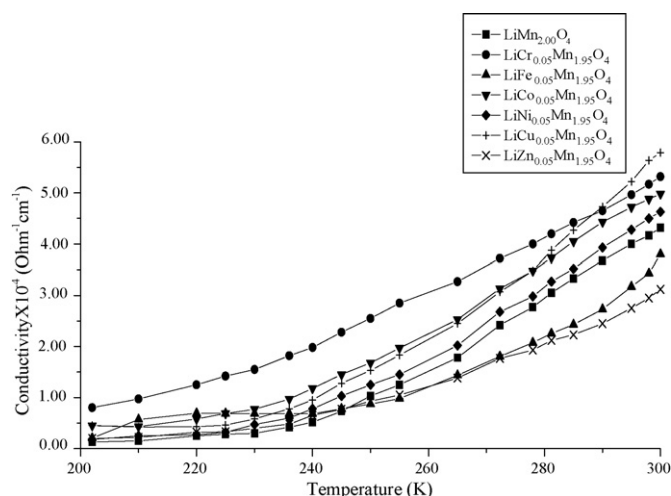
Table 3
Conductivity values of various samples evaluated at room temperature

Samples	Conductivity of the samples annealed at 873 K (ohm^{-1} cm^{-1} $\times 10^{-4}$)	Conductivity of the samples annealed at 1073 K (ohm^{-1} cm^{-1} $\times 10^{-4}$)
$LiMn_2O_4$	3.47	4.17
$LiCr_{0.05}Mn_{1.95}O_4$	4.96	5.17
$LiFe_{0.05}Mn_{1.95}O_4$	3.27	3.43
$LiCo_{0.05}Mn_{1.95}O_4$	3.69	4.88
$LiNi_{0.05}Mn_{1.95}O_4$	4.45	4.50
$LiCu_{0.05}Mn_{1.95}O_4$	5.13	5.64
$LiZn_{0.05}Mn_{1.95}O_4$	2.54	2.95

be an n-type semiconductor [14]. Cr^{3+} is a d^3 system with all the electrons in the t_{2g} orbital, whereas Mn^{3+} is a d^4 system with three electrons in the t_{2g} orbital and one in the e_g orbital [25] as shown in Fig. 8. Similarly, the electronic configuration of Co^{2+} is t_{2g}^4 and e_g^2 and Ni^{2+} has an electronic configuration of t_{2g}^6 and e_g^2. Thus, there are two electrons in the e_g orbital in case of both Co^{2+} and Ni^{2+}. The increase in conductivity is due to the formation of 'holes' as the d^3 system of the dopants replaces the d^4 system of Mn^{3+}.

Conductivity decreases for both Fe^{3+} and Zn^{2+} doped $LiMn_2O_4$ (Table 3). Fe^{3+} has a d^5 system with three electrons in the t_{2g} orbital and two electrons in the e_g orbital. Doping of Fe^{3+} in place of Mn^{3+} may have caused a reduction in the number of available hopping sites and in the number of hopping electrons, which results in a decrease in electrical conductivity for Fe^{3+} doped $LiMn_2O_4$. Similarly, Zn is doped as Zn^{2+} which has a d^{10}
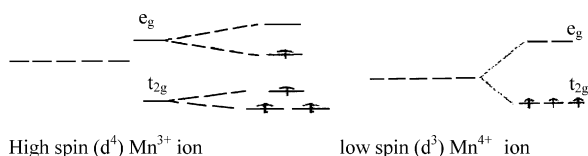

Fig. 8. Electronic arrangements in d orbital of Mn^{3+}/Mn^{4+}.

electronic configuration and there are no electrons available for hopping as the d orbital is completely filled. Further, some of the Mn^{3+} changes into Mn^{4+} to maintain the electroneutrality of the system. As Mn^{3+} is a small polaran carrier in this system, a decrease in their number will lead to a decrease in conductivity.

4. Conclusions

$LiMn_2O_4$ and its derivatives with crystallite sizes of 36–68 nm can be prepared by the sol–gel method. The crystallinity, particle size and lattice parameter (a) increase with increase in annealing temperature. Results from XRD and FTIR analyses reveal the formation of single-phase compounds and that the dopants have preserved the cubic crystal structure of $LiMn_2O_4$. $LiMn_2O_4$ is a semiconductor and its conductivity increases with increase in temperature and also with substitution of Cr^{3+}, Fe^{3+}, Co^{2+}, Ni^{2+}, Cu^{2+} and Zn^{2+} at the Mn^{3+} sites.

References

[1] J.H. Fendler, Nanoparticles and Nanostructured Films, Wiley–VCH, New York, 1998.
[2] A. Hagfeldt, M. Gratzel, Chem. Rev. 95 (1989) 49.
[3] G. Hodes, Y. Golan, D. Behar, Y. Zhang, B. Alperson, I. Rubinstein, Nanoparticles and Nanostructured Films, Wiley–VCH, New York, 1998.
[4] P.V. Kamat, Nanoparticles and Nanostructured Films, Wiley–VCH, New York, 1998, p. 207.
[5] J.M. Tarascon, W.R. McKinnon, F. Coower, T.N. Bowmer, G. Amatucci, D. Guyomard, J. Electrochem. Soc. 141 (1994) 1421–1431.
[6] M.R. Mancini, L. Petrucci, F. Ronci, P.P. Prosini, S. Passerini, J. Power Sources 76 (1998) 91–97.
[7] K.T. Hwang, W.S. Um, H.S. Lee, J.K. Song, K.W. Chung, J. Power Sources 74 (1998) 169–174.
[8] D. Song, H. Ikuta, T. Uchida, M. Wakihara, Solid State Ionics 117 (1999) 151–156.
[9] J.H. Choy, D.H. Kim, C.W. Kwon, S.I. Hwang, Y.I. Kim, J. Power Sources 77 (1999) 1–11.
[10] P. Lucas, C.A. Angell, J. Electrochem. Soc. 147 (2000) 4459–4463.
[11] P.V. Kamat, Prog. React. Kinet. 19 (1994) 277.
[12] J. Guan, M. Liu, Solid State Ionics 110 (1998) 21–28.
[13] G. Li, A. Yamada, Y. Fukishima, K. Yamaura, T. Saito, T. Endo, H. Azuma, K. Sekai, Y. Nishi, Solid State Ionics 130 (2000) 221–228.
[14] S.W. Lee, S.Y. An, I.B. Shin, C.S. Kim, (Eds.) Adv. Nanomaterials Nanodevices (2002) 801–811.
[15] M.G. Lazarraga, S. Mandal, J. Ibanez, J.M. Amarilla, J.M. Rojo, J. Power Sources 115 (2003) 315–322.
[16] Y. Ito, Y. Idemoto, Y. Tsunoda, N. Koura, J. Power Sources 119–121 (2003) 733–737.
[17] C.J. Curtis, J. Wang, D.L. Schutz, J. Electrochem. Soc. 151 (2004) A590–A598.
[18] G.S. Rohrer, Structure and Bonding in Crystalline Materials, Cambridge University Press, UK, 2001, pp. 472–473.
[19] R.S. Liu, C.H. Shen, Solid State Ionics 157 (2003) 95–100.
[20] H.W. Chan, J.G. Duh, S.R. Sheen, J. Power Sources 115 (2003) 110–118.
[21] G.M. Song, Y.J. Wang, Y. Zhou, J. Power Sources 128 (2004) 270–277.
[22] W.J. Moore, Seven Solid States, W.A. Benjamin, New York, 1967, p. 78.
[23] J. Marzec, K. Sweirzek, J. Przewoznick, J. Molenda, D.R. Simon, E.M. Kelder, J. Schoonman, Solid State Ionics 146 (2002) 225–237.
[24] I. Vitioo, Ph.D. Thesis, University of Latvia, Latvia, Synthesis, Structure, Conductivity and Electrode Properties for Some Double Disulphates, Silicates and Lithium Manganese Oxide, 1999.
[25] Y. Shin, Ph.D. Thesis, University of Taxas, Austin, Capacity Fading Mechanisms and Origin of the Capacity above 4.5 V of Spinel Lithium Manganese Oxide, 2003.